J Mar Sci Technol (2016) 21:479–492
DOI 10.1007/s00773-016-0370-5

ORIGINAL ARTICLE

Two degree of freedom flow-induced vibration of cylindrical structures in marine environments: frequency ratio effects

Xiangxi Han[1,2] · Wei Lin[2] · Xiaojun Zhang[3,4] · Youhong Tang[4] · Chengbi Zhao[2]

Received: 27 November 2014 / Accepted: 11 February 2016 / Published online: 23 February 2016
© JASNAOE 2016

Abstract The flow-induced vibration of a cylindrical structure is a very common problem in marine environments such as undersea pipelines, offshore risers, and cables. In this study, the vortex-induced vibration (VIV) of an elastically mounted cylinder at a low Reynolds number is simulated by a transient coupled fluid–structure interaction numerical model. Considering VIV with low damping ratio, the response, hydrodynamic forces, and vortex shedding modes of the cylinder is systematically analyzed and summed up the universal rule under different frequency ratios. On the basis of the analysis, we find that the frequency ratio α is a very important parameter. It decides the locked-in, beat, and phase-switch phenomena of the cylinder, meanwhile, it also influence the vortex mode of the cylinder. The trajectory of the two degrees of freedom (2 DOF) case at different natural frequency ratios is discussed, with most trajectories having a "figure of 8" shape and a few having a "crescent" shape. A fast Fourier transformation technique is used to obtain the frequency characteristics of the vibration of the cylindrical structure. Using the 2 DOF cylinder model in place of the 1 DOF model presents several advantages in simulating the nonlinear characteristics of cylindrical structures, including the capacity to model the crosswise vibration generated by in-line vibration.

Keywords Fluid–structure interaction · Vortex-induced vibration · System coupling

List of symbols

$m^* = m/m_d$	Ratio of oscillating mass over displaced mass
$\zeta = \delta/2\pi$	Damping ratio
$f_n = \frac{1}{2\pi}\sqrt{\frac{k}{m+m_a}}$	Natural frequency of elastic cylinder in still water
$m_a = \rho\pi D^2/4$	Added mass in still water
$U^* = U/(f_n D)$	Reduced velocity in water
f_s	Vortex shedding frequency of elastic cylinder
$St = f_0 D/U$	Strouhal number in still water
$Re = UD/\nu$	Reynolds number
f_0	Vortex shedding frequency of fixed cylinder
$\alpha = f_n/f_0$	Frequency ratio

1 Introduction

The flow-induced vibration of a cylindrical structure is a very common problem in marine environments such as undersea pipelines, offshore risers, and cables, which has

Electronic supplementary material The online version of this article (doi:10.1007/s00773-016-0370-5) contains supplementary material, which is available to authorized users.

✉ Youhong Tang
youhong.tang@flinders.edu.au

✉ Chengbi Zhao
tccbzhao@scut.edu.cn

[1] College of Mechanical and Marine Engineering, Qinzhou University, Guangxi 535000, China

[2] Department of Naval Architecture and Ocean Engineering, School of Civil Engineering and Transportation, South China University of Technology, Guangdong 510641, China

[3] Department of Engineering Mechanics, Beijing University of Technology, Beijing 100124, China

[4] Centre for Maritime Engineering, Control and Imaging, School of Computer Science, Engineering and Mathematics, Flinders University, Adelaide 5042, Australia

arouse many scholars extensively study in recent decades. The research of vortex-induced vibration (VIV) for the design of the marine structure is very important [1]. The VIV is a typical fluid–structure interaction (FSI) problem. The fluid force generated by the vortex around the riser makes the riser vibrate; on the other hand, the oscillating riser also affects the flow field around it. The general process of FSI is like this.

Early VIV research mainly is the study of the one degree of freedom (1 DOF) vibration of a circular cylinder, that is to say, only allow cylindrical cylinder transverse vibration. Feng [2], Brika and Laneville [3, 4], Anagnostopoulos [5], Khalak and Williamson [6] are just a few of the contributing researchers. The content of the VIV for different aspects have been well documented in several overviews, such as those of Sarpkaya [7], Williamson and Govardhan [8, 9], Bearman [10], Okajima [11], Wu et al. [12]. However, the study of VIV considering the two degrees of freedom (2 DOF) is not as much as the 1 DOF. Research into the 2 DOF VIV of a circular cylinder is relatively rare. Jeon and Gharib [13] studied the vortex wake for the 1 and 2 DOF VIV of a circular cylinder, and reported that even a small stream-wise motion can inhibited the formation of 2P (two pair) vortex. Jauvtis and Williamson [14] studied the 2 DOF VIV of a circular cylinder at low mass ratio and reported a new response branch, the "super-upper" branch, which occurred when the mass ratios were reduced below $m^* = 6$. In the "super-upper" branch, the transverse amplitudes of the cylinder vibration can be 1.5 times of the cylinder diameter. Guilmineau and Queutey [15] studied the fluid around an elastically mounted rigid cylinder which is only allowed transverse vibration with low mass-damping. Vortex shedding around the cylinder was investigated numerically by the SST k–ω model. Dahl et al. [16] conducted 2 DOF tests on an elastically mounted rigid cylinder which is allowed transverse and stream–wise vibration at $Re = 11{,}000$–$60{,}000$. In their experiment, the mass ratios were less than 6.0, and the natural frequency ratios of the in-line to transverse varied from 1.0 to 1.9. They reported that the maximum transverse amplitude exceeded 1.35D (where D is the cylinder diameter), whereas the stream-wise response reached 0.6D. When the cylinder was in the largest amplitude response, the cylinder moved along a crescent-shaped orbital trajectory. Placzek et al. [17] reported the result on the cylinders forced or free oscillating in low Reynolds number flow and analyzed the vortex shedding modes related to the frequency response. Bahmani and Akbari [18] investigated the basic characteristics of the dynamic response and vortex shedding on an elastically mounted circular cylinder in laminar flow. Bao et al. [19] reported that the VIV of the isolated and tandem elastically mounted cylinders which were allowed 2 DOF vibration at a series of the natural frequency ratio of the in-line to transverse. Kang and Jia [20] used the experiment to investigate 1 and 2 DOF VIV of a cylinder. A "double peak" phenomenon was found within the range of the reduced velocities tested, moreover, a "2T" wake appeared in the vicinity of the second peak in the 2 DOF VIV experiment, and the trajectory of cylinder exhibited a reverse "C" shape, i.e., a "new moon" shape.

Despite the large number of studies [2–6, 17, 18] dedicated to the VIV of a cylinder vibrating in the transverse direction, there is a little research [13, 14, 16, 19, 20] that also allows the cylinder to vibrate in the in-line direction, with some researchers studying the law of synchronization and the amplitude of vibration in the 2 DOF case [13, 16, 20] and some researchers investigating the regime of synchronization, amplitude, and wake pattern of the isolated and tandem elastically mounted cylinders which are allowed 2DOF vibration at a series of the natural frequency ratio of the in-line to transverse [19]. However, the vortex pattern, trajectory, frequency characteristics and so on have not been investigated with varying frequency ratios $\alpha = f_n/f_0$. Moreover, the VIV of an elastic cylinder has a strongly nonlinear quality. There have been a few nonlinear analyses of phenomena such as locked-in, beat, and phase-switch. From Table 1, it can be seen that most of the literatures investigate the VIV in 1 and 2 DOF with variable mass, damping, Reynolds number, reduced velocity produced by different velocity flow and the in-line to the transverse natural frequency ratio f_{nx}/f_{ny}. Only a small amount of literature [17] studied on the VIV of the circular cylinder with the frequent ratio, but it was the study of the forced oscillations of a cylinder, and only considering transverse vibration. To the best of our knowledge, the frequency characteristics of the vibration of a cylindrical structure in 1 and 2 DOF cases have not been analyzed with varying frequency ratios and there is little discussion on the nonlinear phenomena of bifurcation in VIV and the difference in nonlinear phenomena between VIV with 1 and 2 DOF.

The present work is to study 2 DOF VIV of an elastically mounted cylinder for the varying frequency ratio. The response, hydrodynamic forces, vortex shedding modes and trajectory of the cylinder are systematically analyzed and summed up the universal rule under different frequency ratios. The nonlinear phenomena such as "lock-in", "phase-switch", "beat" are analyzed at different frequency ratios, and the critical point of each nonlinear phenomenon is discussed. Finally, the frequency characteristics of the elastically mounted cylinder is also analyzed at different frequency ratios.

Table 1 The study of parameters in relevant publications

Parameters studied	References
Investigate numerically the dynamics and fluid forcing on an elastically mounted rigid cylinder with a variety of reduced velocity U^*, constrained to oscillate transversely to a free stream	[15]
Forced oscillations characterized by the frequency ratio $\alpha = f_0/f_s$ and the amplitude A	[17]
2 DOF VIV on isolated and tandem cylinders with a variety of the in-line to the transverse natural frequency ratio, f_{nx}/f_{ny}	[19]
The response of an elastically mounted rigid cylinder at low mass damping constrained to oscillate transversely to a free stream with a variety of reduced velocity U^*	[21]
The response of a circular cylinder experiencing VIV in the stream-wise direction and the resulting wake field for a range of reduced velocities in the Reynolds number range 450–3700	[22]
The response of an elastically mounted cylinder, which is free to move in 2 DOF in a fluid flow with a range of reduced velocities and mass ratio	[23]
The VIV of an elastically supported circular cylinder in water with reduced velocity from 2 to 12, damping factors from 0.002 to 0.4, and mass ratios from $\pi/2$ to $\pi/17$	[24]
An experimental and numerical investigation of a 2 DOF VIV of a flexibly mounted circular cylinder with a variety of the in-line to the transverse natural frequency ratio, f_{nx}/f_{ny}	[25]
The effect of blockage on VIV at low *Re* for various values	[26]
A parametric study with respect to the reduced velocity U^* and Reynolds number	[27]

2 Fluid governing equations and transient dynamic analysis

2.1 Fluid governing equations

The two-dimensional, incompressible, Navier–Stokes equations in the Cartesian coordinate, which can be written as follows:

$$\nabla \cdot (\rho \vec{v}) = 0 \tag{1}$$

$$\frac{\partial}{\partial t}(\rho \vec{v}) + \nabla \cdot (\rho \vec{v}\vec{v}) = -\nabla p + \nabla \cdot (\tau) + \vec{F} \tag{2}$$

where p is the static pressure, τ is the stress tensor (described below), and $\vec{F}$ are the external body forces and $\vec{v}$ is the velocity vector. For the two-dimensional, incompressible, Navier–Stokes equations, $\vec{v} = [u, v]$. The large eddy simulation (LES) method is employed for the solution of Eq. 2.

The stress tensor τ is given by

$$\tau = \mu(\nabla \vec{v} + \nabla \vec{v}^T) \tag{3}$$

where μ is the molecular viscosity.

2.2 Transient dynamic theory

The basic equation of an elastically mounted cylinder can be expressed as follows:

$$m\{u\} + c\{\dot{u}\} + k\{u\} = \{F(t)\} \tag{4}$$

where m is the mass of the cylinder, c is the damping, k is the stiffness of the elastically mounted cylinder, $\{u\}\{\dot{u}\}\{u\}\{F(t)\}$ are respectively the acceleration vector, the velocity vector, the displacement vector and the load vector of the cylinder. The Newmark method is employed to solve the Eq. 4.

According to the Eq. 4, the motion equation of the elastically mounted cylinder in the form of dimensionless can be written as follow:

$$u_x + 2\zeta f_n \dot{u}_x + f_n^2 u_x = F_d/m \tag{5}$$

$$u_y + 2\zeta f_n \dot{u}_y + f_n^2 u_y = F_l/m \tag{6}$$

where u_x and u_y are respectively the displacement of the cylinder in the x and y directions, ζ is the damping ratio of the elastically mounted cylinder system and is set to 0.01, f_n is the natural frequency of the cylinder in still water, F_d and F_l are the drag and lift force per unit of length of the cylinder respectively, and m is the mass of the cylinder.

The drag coefficient and lift coefficient are written as follows:

$$C_d = \frac{2F_d}{\rho U^2 D} \tag{7}$$

$$C_l = \frac{2F_l}{\rho U^2 D} \tag{8}$$

where U is the inlet velocity and D is the diameter of the cylinder.

2.3 Diffusion-based smoothing method

For diffusion-based smoothing, the mesh motion is governed by the diffusion equation.

$$\nabla \cdot (\gamma \nabla \vec{u}) = 0 \tag{9}$$

where $\vec{u}$ is the mesh displacement velocity. The boundary conditions for Eq. 9 are obtained from the user-prescribed or computed (6 DOF) boundary motion. On deforming

boundaries, the boundary conditions are such that the mesh motion is tangent to the boundary (i.e., the normal velocity component vanishes). The Laplace equation in Eq. 9 describes how the prescribed boundary motion diffuses into the interior of the deforming mesh. The diffusion coefficient γ in Eq. 9 can be used to control how the boundary motion affects the interior mesh motion. A constant coefficient means that the boundary motion diffuses uniformly throughout the mesh. With a non-uniform diffusion coefficient, mesh nodes in regions with high diffusivity tend to move together (i.e., with less relative motion).

For diffusivity based on boundary distance, the diffusion coefficient γ is equal to the following formula.

$$\gamma = \frac{1}{d^{\theta}} \tag{10}$$

where d is a normalized boundary distance. The boundary-distance-based diffusion Eq. 10 controls how the boundary motion diffuses into the interior of the domain as a function of boundary distance. Decreasing the diffusivity away from the moving boundary causes those regions absorb more mesh motion, and results better mesh quality near the moving boundary. This is particularly helpful for a moving boundary that has pronounced geometrical features (such as sharp corners) along with a prescribed motion that is predominantly rotational.

The diffusion coefficient γ is adjusted by the diffusion parameter θ. A range of 0–2 has been shown to be of practical use. A value of 0 (the default value) specifies that $\gamma = 1$ and yields a uniform diffusion of the boundary motion throughout the mesh. A higher value of θ preserves a larger region of the mesh near the moving boundary, and cause the region away from the moving boundary to absorb more motion.

2.4 FSI

At an iterative process of every time step, firstly, Eqs. 1, 2 are solved to obtain the drag and lift forces of the cylinder; secondly, the drag and lift forced are substituted into the Eqs. 5, 6, and then the response of the cylinder is obtained by using the method of Newmark to solve the Eqs. 5, 6; finally, the mesh is updated with the diffusion-based smoothing method based on the response of the cylinder. The interactive process is repeated iteratively, so that the interactions between fluid and the cylinder can be calculated correctly.

2.5 The connection of each module

The VIV behaviour of a circular cylinder is simulated by a transient coupled FSI numerical model using the combination of FLUENT and ANSYS transient structure platforms. The well-designed FSI solution scheme provides tight integration between hydrodynamics and structural physics, offering a flexible, advanced structure–fluid analysis tool. The connections of each module are shown in Fig. 1. The geometry module provides a geometric model for the transient structure solver and the FLUENT solver. Coupled simulations begin with the execution of the ANSYS transient structure and FLUENT solvers. The system coupling solver acts as a coupling master process to which the transient structure solver and FLUENT solvers connect. Once that connection is established, the solvers advance through a sequence of pre-defined synchronization points (SP). At each of these SPs, the FLUENT solver transfers the fluid dynamic loads data to the transient structure solver based on the system coupling solver; in turn, the transient structure solver transfers the structure response data to the FLUENT solver also based on the system coupling solver. Finally, the mesh is updated with the diffusion-based smoothing method based on the response of the cylinder. The coupled simulation proceeds in time during the outer loop. Staggered iterations are repeated until a maximum number of stagger iterations is reached or until the data transferred between solvers and all field equations have converged. The adoption of implicit coupling iteration ensures that fluid and structure solution fields are consistent with each other at the end of each multi-field step, leading to improved numerical solution stability.

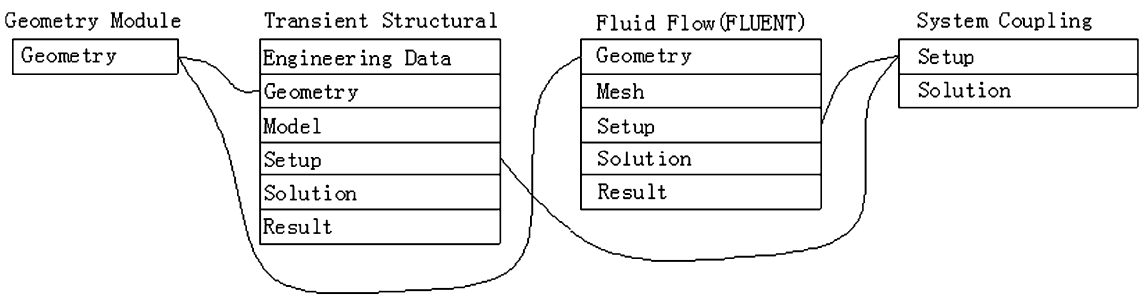

Fig. 1 The connections of each module

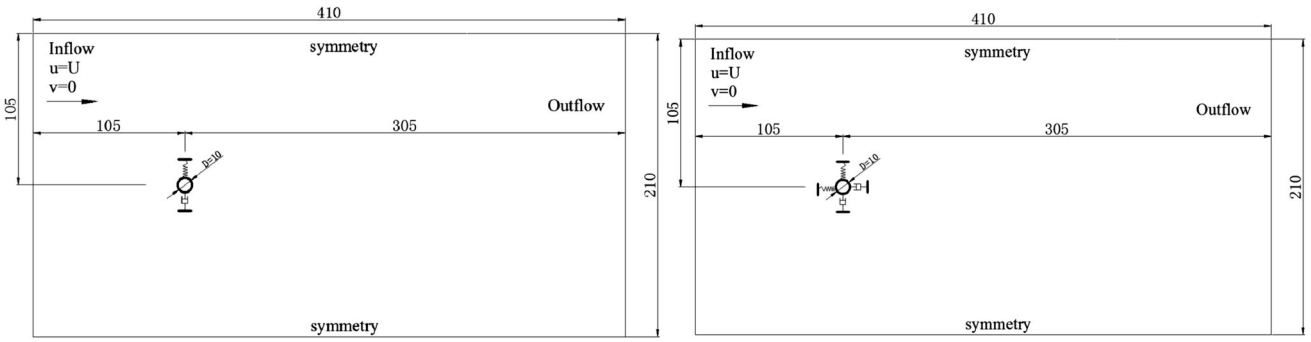

Fig. 2 Schematic of (*left*) 1 DOF and (*right*) 2 DOF computational domains

3 Computational domain and mesh

In this section, we describe the calculation model of this research. For 1 DOF model, we only allow cylindrical cylinder to move in the transverse direction. For 2 DOF model, we allow cylindrical cylinder to move in the transverse and stream-wise direction (as shown in Fig. 2). The inlet velocity is set to 0.02 m/s. The right side boundary is set to an outflow boundary condition ($\frac{\partial u}{\partial x} = 0$; $\frac{\partial v}{\partial x} = 0$). The upper and lower side boundaries are set to the symmetry boundary condition ($\frac{\partial u}{\partial y} = 0$; $v = 0$). Time step is 0.01. For the simulation task, the common goal of grid design is to provide sufficient grid nodes to obtain sufficient flow field resolution and then we can accurately simulate the flow field. Therefore, near the cylinder, we adopt relatively fine mesh to express severe changes of flow field around the cylinder, with the aim of achieving an accurate solution. Flow field away from the cylinder is relatively stable, we adopt relatively coarse mesh to express its flow field and the coarse mesh can deal with the grid deformation for the cylinder movement. The thickness of the first layer grid must meet the condition that $y^+ = \frac{y}{\mu}\sqrt{\rho\tau_w} \approx 1$, where y is the distance from the wall to the cell center, μ is the molecular viscosity, ρ is the density of the water, and τ_w is the wall shear stress. On the cylindrical surface, we arranged 80 nodes. According to the above grid partitioning strategy, the whole flow field grid consists of 11,600 quadrilateral elements. The mesh near the circular cylinder is shown in Fig. 3.

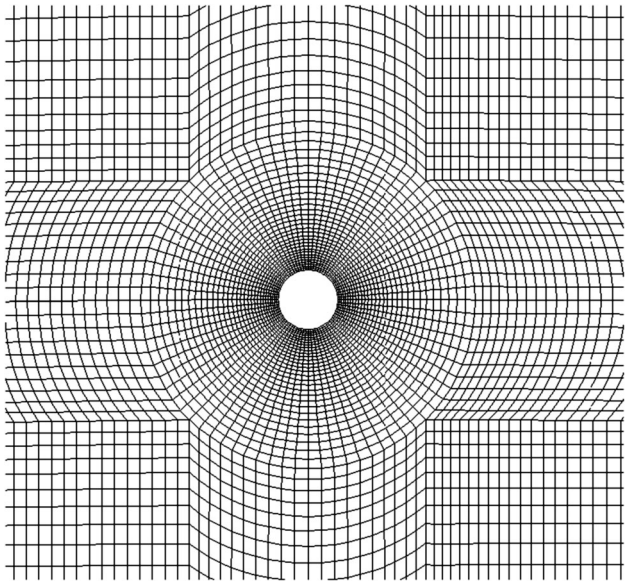

Fig. 3 Mesh near the circular cylinder

4 Validation tests

We use the grid and time step determined in the previous section to solve a test case of a fixed circular cylinder in cross-flow at $Re = 200$. Table 2 presents the comparison of our predictions with results found in the literature [28–30]. The drag and lift coefficients and the Strouhal number are obtained by analyzing their time history over an interval of 30 vortex shedding periods. The drag coefficient is the mean value of the in-line non-dimensionalized force and the lift coefficient is the maximum value of the non-dimensionalized transverse load. Our results are in good agreement with the previously published results [21–23].

Table 2 Fixed cylinder at $Re = 200$

Fixed cylinder	Average of Cd	Amplitude of Cl	St
Halse [28]	1.35	0.62	0.196
Liu et al. [29]	1.31	0.69	0.192
Li et al. [30]	1.34	0.69	0.192
Present result	1.315	0.68	0.19

5 VIV of the cylinder with 2 DOF

The VIV of an elastically mounted rigid cylinder is nonlinear. The fluid force generated by the vortex around the cylinder makes the cylinder vibrate; in turn, the oscillating cylinder also affects the flow field around it, eventually flow field changes the induced forces on the cylinder and hence the cylinder responses. In order to systematically study the effect of frequency ratio α for the VIV characteristics of an elastically mounted rigid cylinder, the frequency ratio $\alpha = f_n/f_0$ ranges from 0.3 to 2.0 at intervals of 0.1 are used. In our study, the Reynolds number value is equal to 200, the damping ratio $\zeta = 0.01$, and the mass ratio $m^* = \frac{4}{\pi}$.

5.1 Force time history and two-direction response

Figure 4 shows time history of the drag and lift forces, the cross-flow and stream-wise displacements of an elastically mounted rigid cylinder. Through Fig. 4, when the frequency ratios are at big values, for example $\alpha = f_n/f_0 = 2$, the time history are very similar to those of the fixed cylinder (as shown in Fig. S1 in the supplementary material). That is because the fixed cylinder can be seen as an elastic cylinder with infinite stiffness. When α is at small value, some interesting VIV characteristics can be observed. When t α varies from 0.3 to 0.5, the drag coefficient mean value is smaller than that of the fixed cylinder. When $\alpha > 0.5$, the mean value of the drag coefficient increases. When α varies from 0.3 to 2.0, the amplitude of the drag coefficient first increases gradually, and then decrease gradually.

When α varies from 0.3 to 2.0, the lift coefficient and the transverse displacement curves show an obvious phenomenon: the phase between the lift coefficient and the transverse displacement undergoes an interesting "sudden" jumping from the "out-of-phase" to the "in-phase" mode, which is called the "phase-switch" phenomenon. When α is between 0.3 and 0.5, the lift coefficient and transverse displacement are in the "out-of-phase" stage, and when α is between 0.8 and 2.0, both lift coefficient and transverse displacement are in the "in-phase" stage. Between "out-of-phase" and "in-phase", the lift coefficient has an obvious characteristic: its amplitude becomes very small. As shown in Fig. 4, when $\alpha = 0.6$–0.7, the amplitude of the lift coefficient is very small.

When α is 0.5, compared with the amplitude of $\alpha = 0.4$, the transverse vibration amplitude suddenly increases, marking the beginning of the "lock-in" phenomenon. At this time the frequency of vortex shedding is locked into the natural frequency of the cylinder.

When α is between 1.2 and 1.4, the lift and drag coefficient and the transverse displacement curve clearly shows two kinds of frequencies influence on each other, known as the "beat" phenomenon. The lift coefficient of amplitude is large at this time, showing that the intensity of vortex is very great. From "no beat" to "beat", the cylinder's lift curve experiences a more disorderly state. As shown in Fig. 4, when α is 1.2, the lift coefficient curve is disorderly.

5.2 Vortex pattern in wake

Figure 5 shows comparisons of the vortex patterns in the wake of the elastically mounted rigid cylinder at different α. The vortex patterns differ with different amplitudes of cylinder motion and α. When α is at a big value (as shown in Fig. 5, $\alpha = 2.0$), the vortex pattern of the elastic cylinder is very similar to that of the fixed cylinder, i.e., a 2S (two single) pattern (Fig. S3). When α is at a small value (as shown in Fig. 5, $\alpha = 0.3$), the vortex pattern is a 2P (two pair) pattern. With the increase of α, the cylinder oscillation begins to affect the vortex pattern in the wake. The transverse distances and stream-wise distances between vortices in the wake begin to change. As shown in Fig. 5, when $\alpha = 0.8$, the spacing between vortices in the stream-wise direction narrows, while the spacing widens in the transverse direction, and then two parallel rows vortices with the blue and red in the near wake appear. When $\alpha = 0.8$–1.1, the vortex pattern forms a double line vortex. The phenomenon of the vortex pattern switch corresponds to the phase-switch of lift coefficient and transverse displacement. When the phase-switch occurs, the vortex pattern switches from "single line" to "double line". The amplitude of the transverse vibration is the reason for the formation of the "double line vortex". The ratio of the vortex transverse displacement and the vortex stream-wise displacement is much greater than that of the fixed cylinder. As α reaches 1.2–2.0, the vortex of transverse displacement gradually decreases and the vortex pattern switches from "double line" to "single line". In general, as the frequency ratio increases, the VIV experiences three interesting processes: phase-switch, locked-in, and beat. In the "lock-in" stage, the vortex shedding modes is mainly double line mode, while in other stage, the vortex shedding are mainly single line mode, and in the case of lower frequency ratios shows 2P wake vortex, in the case of higher frequency ratios show 2S wake vortex.

5.3 Trajectory of the elastically mounted rigid cylinder at different natural frequency ratios

Figure 6 shows the periodical trajectory plot of the elastically mounted rigid cylinder in comparison to the results of different studies [27, 31, 32], in their studies as well as in our study, the Reynolds number value is equal to 200, the

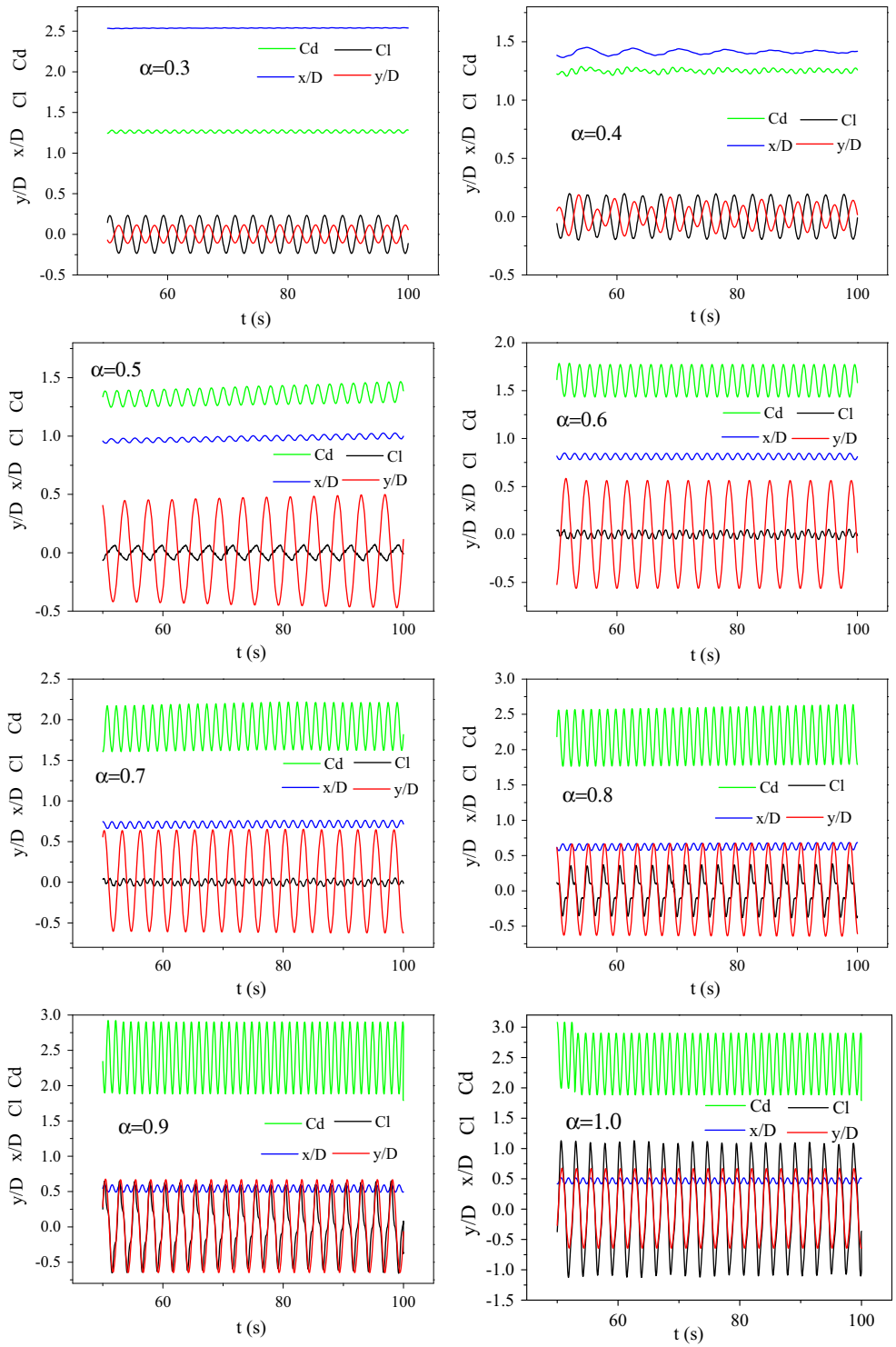

Fig. 4 Time history of the drag and lift forces, the cross-flow and stream-wise displacements of the elastically mounted rigid cylinder

damping ratio $\zeta = 0.01$, the reduced velocity $U^* = 5.0$, and the mass ratio $m^* = \frac{4}{\pi}$, confirming that our predictions are reliable. Figure 7 shows the trajectory of an elastic cylinder for 2 DOF with various α. These trajectories clearly show that the oscillations are self-limiting and similar to a "Fig. 8" shape or a "crescent" shape. With the increment of α, the mean value of the stream-wise direction becomes smaller; meanwhile, the amplitude of the transverse vibration firstly increases and then decreases. Note that the mean value of the vibration in the stream-wise

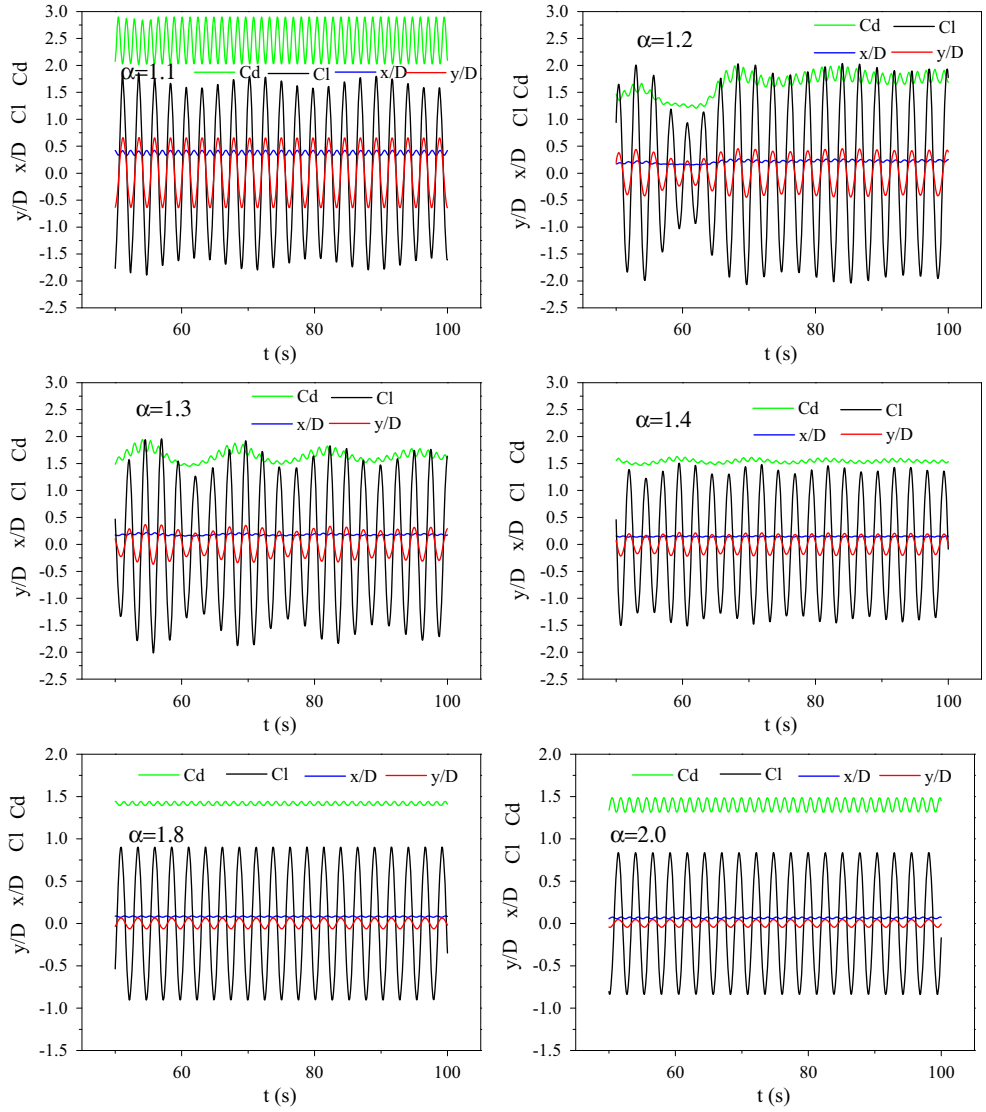

Fig. 4 continued

direction is not zero, because the drag force mean value of the cylinder is not equal to zero. The trajectory in Fig. 7 is from 50 to 100 s, and when $\alpha = 0.4$, the trajectory does not show a "Fig. 8" or a "crescent" shape. The frequency of stream-wise vibration is not twice as great as the frequency of transverse vibration at α. The trajectories of each cycle at each α do not perfectly coincide, because the mean of the stream-wise vibration response and the amplitude is not constant, but fluctuates a little, reflecting the randomness of the VIV.

5.4 Analysis of 2 DOF result

Figure 8 shows the RMS lift coefficient and RMS transverse displacement for various α. When α is at a small value ($\alpha = 0.3$), the RMS lift coefficient of the elastic cylinder is large and the response of the cylinder is weak. With the increase of α, the RMS transverse displacement of the cylinder also increases, but the RMS lift coefficient decreases. When $\alpha = 0.6$, the RMS lift coefficient obtains the minimum value. After that, the RMS lift coefficient begins to increase, reaching its maximum value when $\alpha = 1.2$. When $\alpha > 1.2$, the RMS lift coefficient begins to decrease again. Meanwhile, the RMS transverse displacement reaches its maximum value when α is between 0.8 and 1.1. After that, the RMS transverse displacement begins to decrease. We need to pay attention to that the transverse displacement and the RMS lift coefficient are not direct proportion relationship. However, with the increment of α, the natural frequency of the cylinder in still water is increased, and then the elastic strength of the cylinder is increased. For this reason, the mean stream-wise

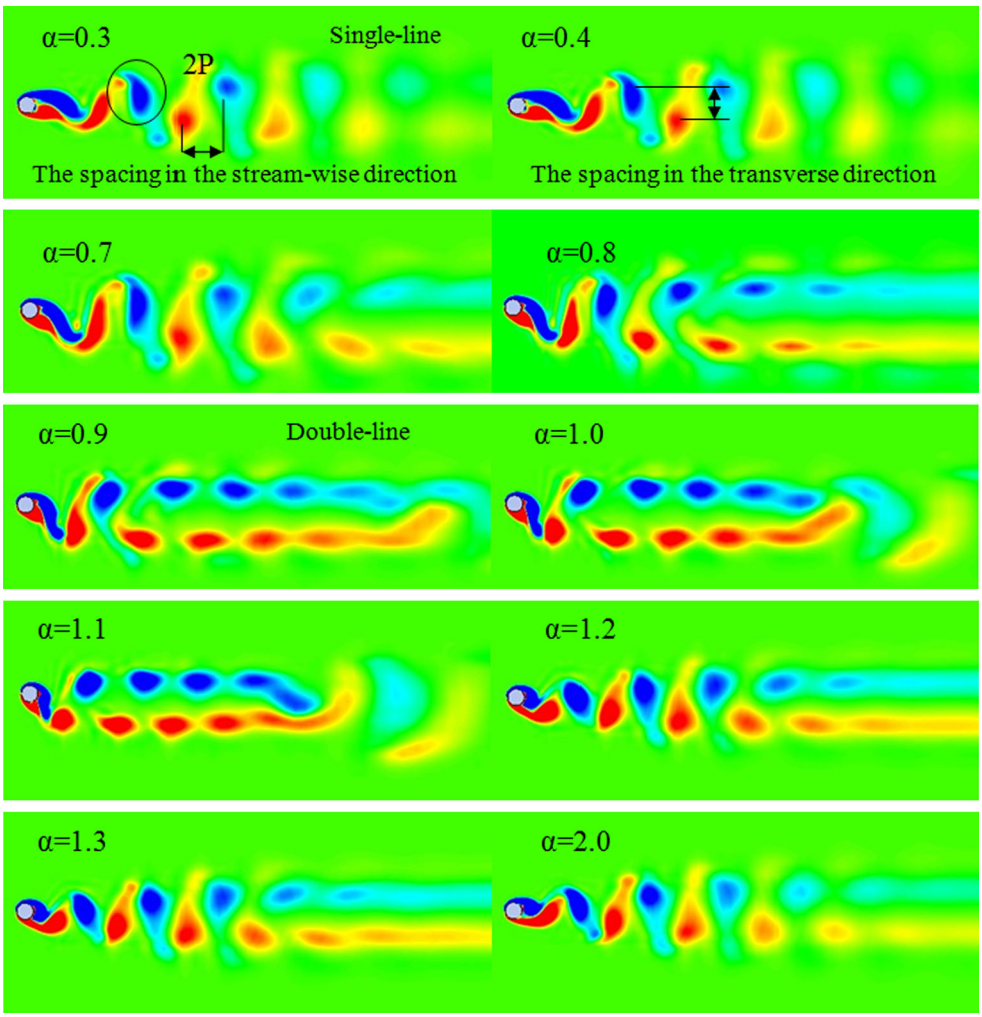

Fig. 5 Comparison of vortex patterns at different frequency ratios

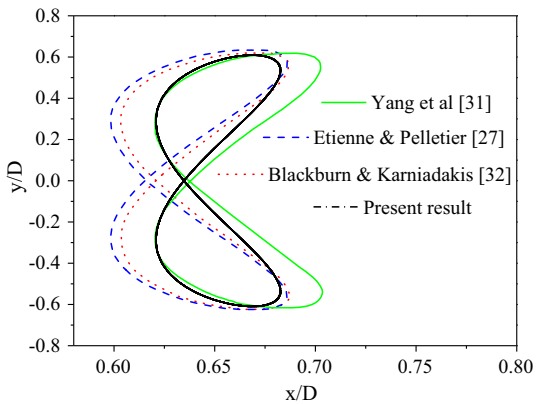

Fig. 6 Comparison of periodical trajectory of elastic cylinder at $U^* = 5$ and $Re = 200$

displacement is not direct proportion relationship. Figure 9 shows the mean drag coefficient and the mean stream-wise displacement for various α. When α is small ($\alpha = 0.3$), the mean drag coefficient of the elastic cylinder is small and the mean stream-wise displacement is large. With the increase of α, the mean drag coefficient of the cylinder increases, but the mean stream-wise displacement of the cylinder decreases. When α ranges from 0.9 to 1.1, the mean drag coefficient reaches its maximum value. After that, the mean drag coefficient begins to decrease, finally reaching the mean drag coefficient of a fixed cylinder. As α increases, the mean stream-wise displacement decreases, finally reaching zero.

6 Comparison of the 1 DOF and 2 DOF cases

Comparison of the mean drag coefficient, the RMS lift coefficient, the mean of stream-wise displacement, the RMS transverse displacement, and the phase difference between the lift coefficient and transverse displacement for the 1 DOF and 2 DOF cases is shown in Figs. 10, 11, 12, 13 respectively. Figure 10 shows the comparison of the mean drag coefficient. The mean drag coefficients of the 1

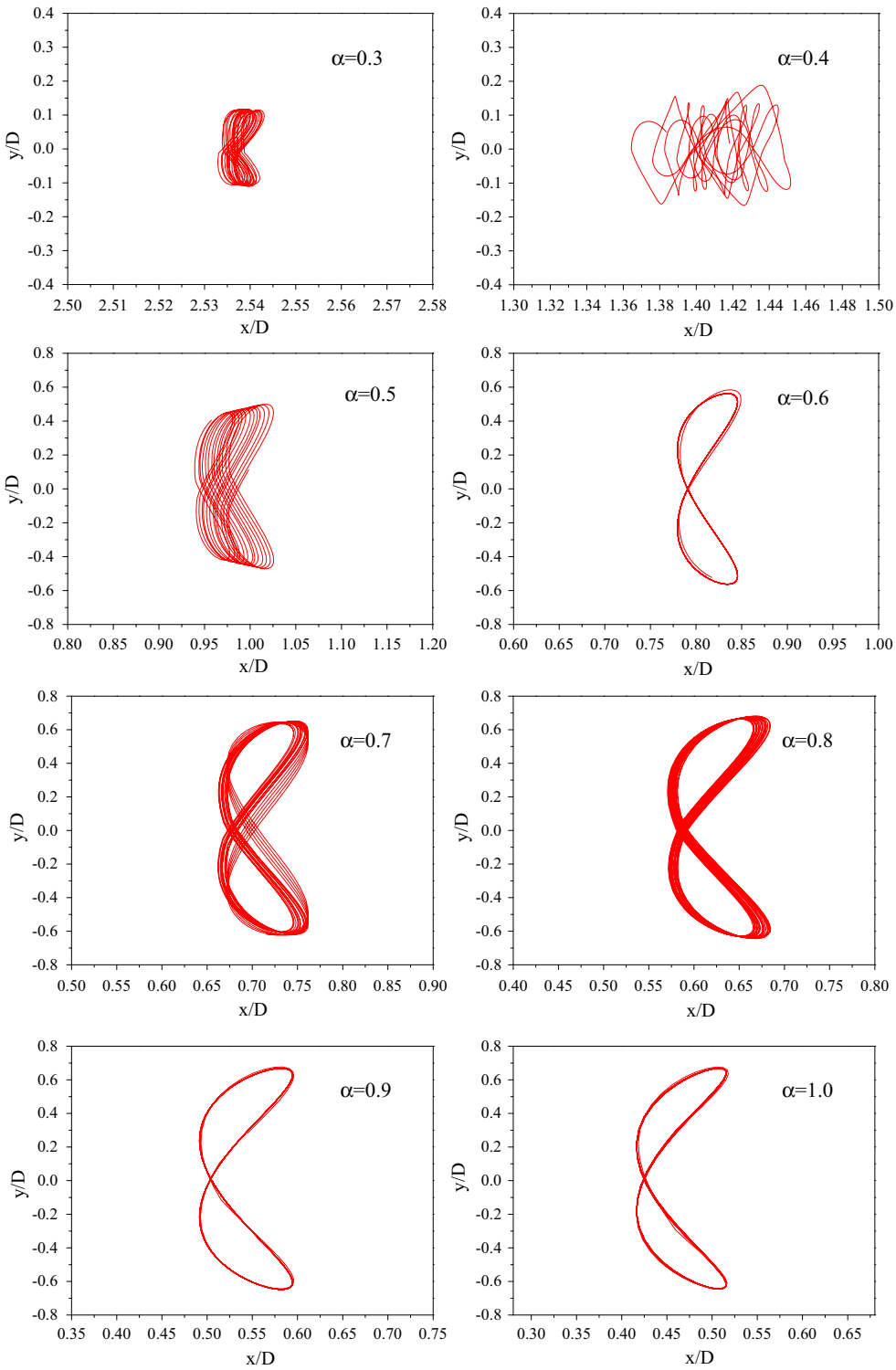

Fig. 7 Trajectory of elastic cylinder for 2 DOF

DOF and 2 DOF cases are almost equal, but the peak value in the 2 DOF case is a little bigger than that in the 1 DOF case. Figure 11 shows the comparison of the RMS transverse displacement. The amplitude of y_r.m.s/D has a higher value for the 2 DOF case than that of the 1 DOF case. The α of the 2 DOF case reaches a peak value that is smaller than the corresponding value of the 1 DOF case. It is evident that the results of the 1 DOF VIV model are only in qualitative agreement with the 2 DOF model, because the stream-wise oscillations, which cannot be captured by 1 DOF model, have an important influence to the transverse vibrations. Figure 12 shows the comparison of the RMS lift

Fig. 7 continued

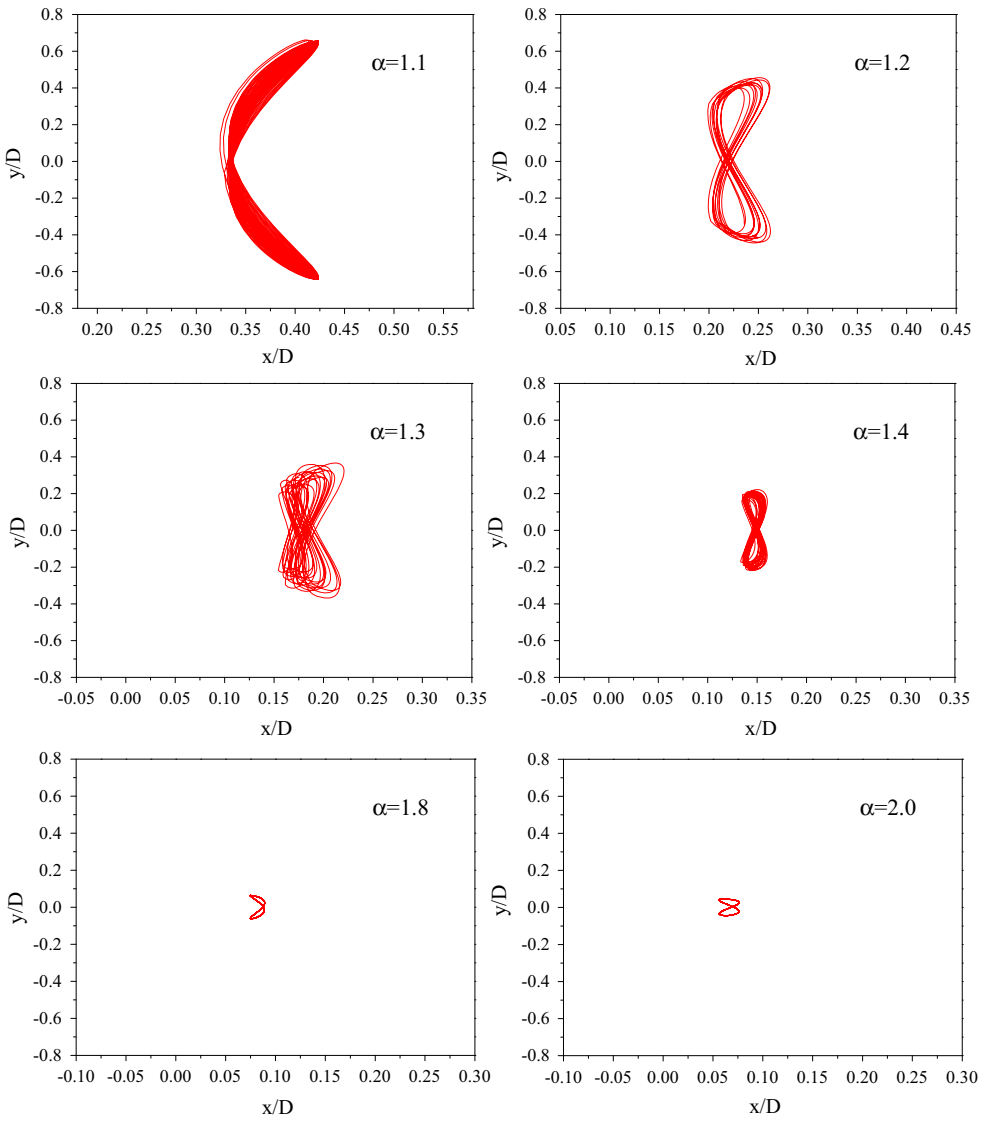

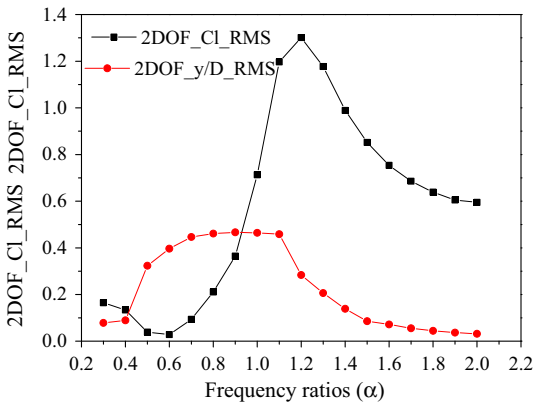

Fig. 8 RMS lift coefficient and RMS transverse displacement for various frequency ratios

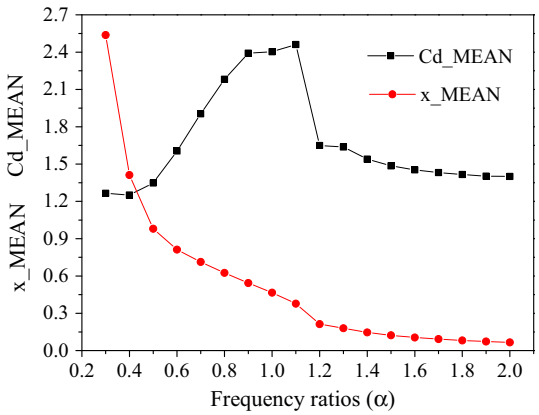

Fig. 9 Mean drag coefficient and mean stream-wise displacement for various frequency ratios

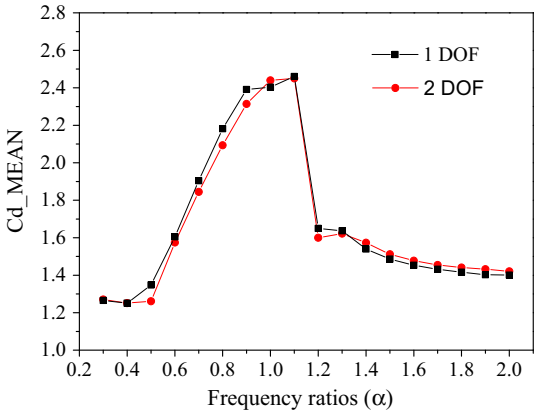

Fig. 10 Comparison of mean drag coefficients

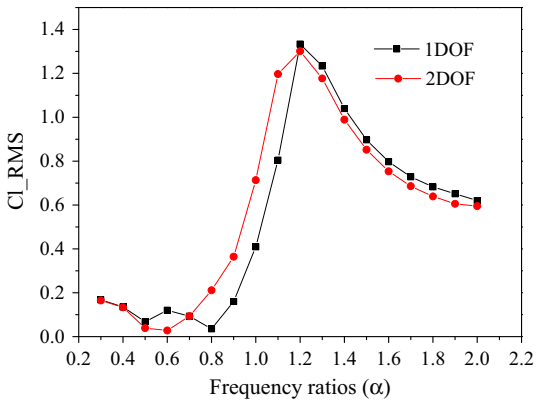

Fig. 12 Comparison of the RMS lift coefficients

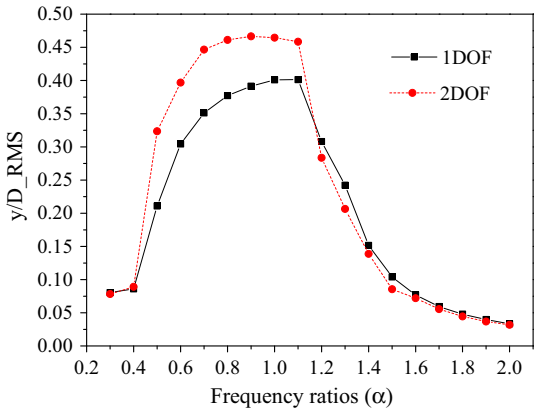

Fig. 11 Comparison of the RMS transverse displacements

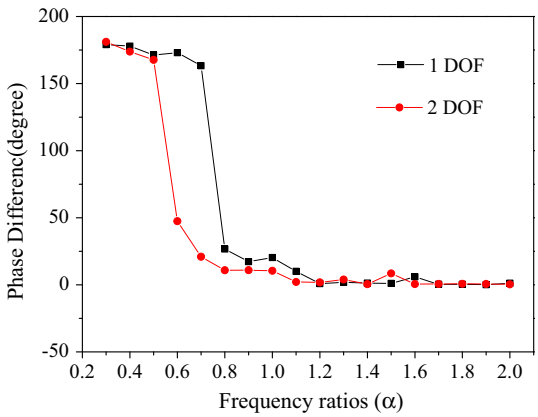

Fig. 13 Comparison of phase differences

coefficient. The peak value of r.m.s Cl is almost the same as that of the 1 DOF case. It is found that α of the 2 DOF case reaches the same value, which is smaller than the corresponding value of the 1 DOF case. In other words, 2 DOF lift coefficient curve changes ahead of the 1 DOF lift coefficient curve. For example, when $\alpha = 0.6$, the RMS lift coefficient obtains the minimum value in the 2 DOF case, but the minimum value is reached $\alpha = 0.8$ in the 1 DOF case, which is later than in the 2 DOF case. Figure 13 shows the comparison of the phase differences between the lift coefficient and transverse displacement. The phase difference undergoes a "sudden" jumping from the "out-of-phase" to the "in-phase" mode. The "phase-switch" phenomenon appears at about $\alpha = 0.5$ in the 2 DOF case but at about $\alpha = 0.7$ in the 1 DOF case, which is also later than that of the 2 DOF case. In both 1 DOF and 2 DOF cases, when "phase-switch" phenomena occur, the pattern begins to change from a single line pattern to the corresponding double line pattern.

To sum up, both 1 DOF case and 2DOF case experience three phenomena: phase-switch, locked-in, and beat, but the "phase-switch" phenomenon appears in the 1 DOF case is later than that of the 2 DOF case with the frequency ratio increasing. In "phase switch" stage, root mean square of lift coefficient reach minimum and the phase difference of the lift coefficient and the lateral displacement response is nearly 180°. In the "lock-in" stage, the root mean square of lateral displacement is larger. Using the 2 DOF cylinder model in place of 1 DOF model presents several advantages in simulating the nonlinear characteristics of cylindrical structures, including the capacity to model the crosswise vibration generated by in-line vibration.

7 Frequency spectral analysis of structural response

To obtain the frequency characteristics of the vibration of the cylindrical structure, a fast Fourier transformation technique is used to transform data from the time domain into the frequency domain to obtain the frequency spectral analysis. The ratios of the vortex shedding frequency and the natural frequency of the elastically mounted rigid cylinder at different α for 2 DOF case are shown in Fig. 14.

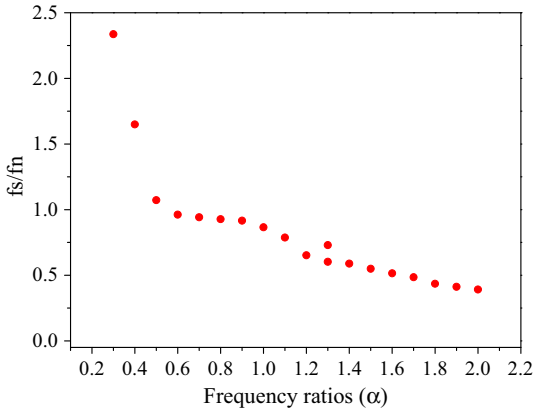

Fig. 14 Ratios of the vortex shedding frequency and the natural frequency of the elastically mounted rigid cylinder at different frequency ratios for 2 DOF case

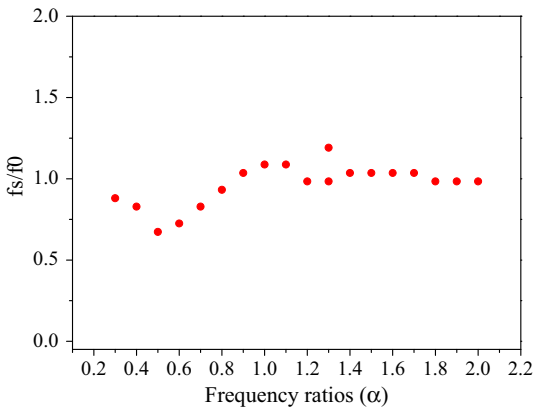

Fig. 15 Ratio of the elastically mounted rigid cylinder vortex shedding frequency and the fixed cylinder vortex shedding frequency at different frequency ratios for the 2 DOF case

As with the 1 DOF (Fig. S5 in the supplementary material) results, The ratios of the vortex shedding frequency and the natural frequency of the elastically mounted rigid cylinder is very large for $\alpha = 0.3$–0.4. When $\alpha = 0.5 \sim 1.1$, the ratios of the vortex shedding frequency and the natural frequency of the elastically mounted rigid cylinder is approximately equal to one, and the vortex shedding frequency is locked into the natural frequency of the elastically mounted rigid cylinder. As α increases, the cylinder undergoes the beat stage, after which the vortex shedding frequency is no longer locked into the cylinder's natural frequency.

The ratios of the elastic cylinder vortex shedding frequency and the fixed cylinder vortex shedding frequency at different α for the 2 DOF case are shown in Fig. 15. The ratio of the elastic cylinder vortex shedding frequency and the fixed cylinder vortex shedding frequency f_s/f_0 tends to 1 for $\alpha = 0.3$. f_s/f_0 gradually increases from $\alpha = 0.5$. From

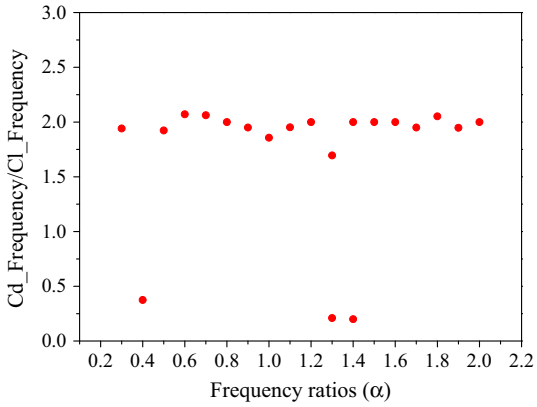

Fig. 16 Ratio of the drag coefficient frequency and the lift coefficient frequency at different frequency ratios for the 2 DOF case

Fig. 14, it can be seen that the elastic cylinder vortex shedding frequency f_s begins to be locked into the natural frequency of the elastically mounted rigid cylinder f_n. According to the analysis above, we make a conclusion that when α is not close to 1, the elastic cylinder vortex shedding frequency f_s is close to the fixed cylinder vortex shedding frequency f_0.

The ratios of the drag coefficient frequency and the lift coefficient frequency at different α for 2 DOF case are shown in Fig. 16. When the elastic cylinder undergoes VIV, the ratio of the drag coefficient frequency and the lift coefficient frequency is not equal to two (the ratio of the drag coefficient frequency and the lift coefficient frequency is equal to two for the fixed cylinder), except during the beat stage.

8 Conclusion

This study presents a numerical simulation study of VIV characteristics on an elastically mounted rigid cylinder with Reynolds number = 200 and damping ratio = 0.01. In this research, the numerical calculation is achieved by combination of the LES method, transient dynamic theory, and dynamic mesh technology. The response, hydrodynamic forces, vortex shedding modes of the cylinder, and the trajectory are systematically analyzed and summed up the universal rule under different frequency ratios, and summarize the basic rule of their time history. The nonlinear phenomena such as "lock-in", "phase-switch", "beat" are analyzed at different natural frequency ratios, and find out the critical point of each nonlinear phenomenon. Both 1 DOF and 2DOF cases experience three phenomena: phase-switch, locked-in, and beat, but the "phase-switch" phenomenon appears in the 1 DOF case is later than that of the 2 DOF case with the frequency ratio increasing. In the "lock-in" stage, the vortex shedding

modes is mainly double line mode, while in other stage, the vortex shedding are mainly single line mode, and in the case of lower frequency ratios shows 2P wake vortex, in the case of higher frequency ratios show 2S wake vortex. In "phase switch" stage, root mean square of lift coefficient reach minimum and the phase difference of the lift coefficient and the lateral displacement response is nearly 180°. In the "lock-in" stage, the root mean square of lateral displacement is larger. In the "beat" stage, the elastic cylinder shows characteristic of the multi-frequency vibration. In some frequency ratio (such as) when the elastic cylinder occur vortex-induced vibration, the relationship between the frequency of drag coefficient and the frequency lift coefficient is not the two times.

The frequency characteristics of the elastically mounted cylinder are also analyzed at different frequency ratios. At a wide range of frequency ratio, $\alpha = 0.5–1.1$, vortex shedding frequency of elastic cylinder locking in the natural frequency of elastic cylinder in still water. By comparing the transverse vibration amplitude, phase-switch, lateral displacement RMS, lift coefficient RMS, the 2 DOF cylinder model presents several advantages over the 1 DOF cylinder model in simulating the nonlinear characteristics of cylindrical structures, including the capacity to model the crosswise vibration generated by in-line vibration.

Acknowledgments This study was supported by a guiding fund for the integration of industry, education and research of Guangdong Province, China (Grant No. 2012B091100132), a middle-aged and young teachers' basic ability promotion project of Guangxi Zhuang Autonomous Region (Numerical simulation research of marine riser vortex-induced vibration), the key discipline of guangxi colleges and universities - automation and machinery manufacturing.

References

1. Anagnostopoulos P, Bearman PW (1992) Response characteristics of a vortex-excited cylinder at low Reynolds number. J Fluids Struct 6:39–50
2. Feng C (1968) The measurement of vortex-induced effects in flow past stationary and oscillation circular and d-section cylinders. M.A.Sc. Thesis. British Columbia, Vancouver, BC
3. Brika D, Laneville A (1993) Vortex-induced vibrations of a long flexible circular cylinder. J Fluid Mech 250:481–508
4. Brika D, Laneville A (1997) Wake interference between two circular cylinders. J Wind Eng Ind Aerod 72:61–70
5. Anagnostopoulos P (1994) Numerical investigation of response and wake characteristics of a vortex excited cylinder in a uniform stream. J Fluids Struct 8:367–390
6. Khalak A, Williamson CHK (1996) Dynamics of a hydroelastic cylinder with very low mass and damping. J Fluids Struct 10:455–472
7. Sarpkaya T (2004) A critical review of the intrinsic nature of vortex-induced vibrations. J Fluids Struct 19:389–447
8. Williamson CHK, Govardhan R (2004) Vortex-induced vibrations. Annu Rev Fluid Mech 36:413–455
9. Williamson CHK, Govardhan R (2008) A brief review of recent results in vortex-induced vibrations. J Wind Eng Ind Aerod 96:713–735
10. Bearman PW (1984) Vortex shedding from oscillating bluff bodies. Annu Rev Fluid Mech 16:195–222
11. Okajima A (1993) Brief review: numerical analysis of the flow around vibrating cylinders. J Wind Eng Ind Aerod 46:881–884
12. Wu X, Ge F, Hong Y (2012) A review of recent studies on vortex-induced vibrations of long slender cylinders. J Fluids Struct 28:292–308
13. Jeon D, Gharib M (2001) On circular cylinders undergoing two-degree-of-freedom forced motions. J Fluids Struct 15:533–541
14. Jauvtis N, Williamson CHK (2004) The effect of two degrees of freedom on vortex-induced vibration at low mass and damping. J Fluid Mech 509:23–62
15. Guilmineau E, Queutey P (2004) Numerical simulation of vortex-induced vibration of a circular cylinder with low mass-damping in a turbulent flow. J Fluid Mech 19:449–466
16. Dahl JM, Hover FS, Triantafyllou MS (2006) Two-degree-of-freedom vortex-induced vibrations using a force assisted apparatus. J Fluids Struct 22:807–818
17. Placzek A, Sigrist JF, Hamdouni A (2009) Numerical simulation of an oscillating cylinder in a cross-flow at low Reynolds number: forced and free oscillations. Comput Fluids 38:80–100
18. Bahmani MH, Akbari MH (2010) Effects of mass and damping ratios on VIV of a circular cylinder. Ocean Eng 37:511–519
19. Bao Y, Huang C, Zhou D, Tu J, Han Z (2012) Two-degree-of-freedom flow-induced vibrations on isolated and tandem cylinders with varying natural frequency ratios. J Fluid Mech 35:50–75
20. Kang Z, Jia LS (2013) An experimental investigation of one- and two-degree of freedom VIV of cylinders. Acta Mech Sin 29:284–293
21. Pan ZY, Cui WC, Miao QM (2007) Numerical simulation of vortex-induced vibration of a circular cylinder at low mass-damping using RANS code. J Fluid Struct 23:23–37
22. Cagney N, Balabani S (2013) Wake modes of a cylinder undergoing free stream wise vortex-induced vibrations. J Fluid Struct 38:127–145
23. Jauvtis N, Williamson CHK (2003) Vortex-induced vibration of a cylinder with two degrees of freedom. J Fluid Struct 17:1035–1042
24. Blevins RD, Coughran CS (2009) Experimental Iinvestigation of vortex-induced vibration in one and two dimensions with variable mass, damping, and Reynolds number. J Fluid Eng 131:101202
25. Srinil N, Zanganeh H, Day A (2013) Two-degree-of-freedom VIV of circular cylinder with variable natural Experimental and numerical investigations. Ocean Eng 73:179–194
26. Prasanth TK, Mittal S (2008) Vortex-induced vibrations of a circular cylinder at low Reynolds numbers. J Fluid Mech 594:463–491
27. Etienne S, Pelletier D (2012) The low Reynolds number limit of vortex-induced vibrations. J Fluids Struct 31:18–29
28. Halse K (1997) On vortex shedding and predictions of VIV of circular cylinders. Ph.D. Thesis. NTNU Trondheim
29. Liu C, Zheng X, Sung CH (1998) Preconditioned multigrid methods for unsteady incompressible flows. J Comput Phys 139:35–57
30. Li T, Zhang J, Zhang W (2011) Nonlinear characteristics of vortex-induced vibration at low Reynolds number. Commun Nonlinear Sci Numer Simul 16:2753–2771
31. Yang J, Preidikman S, Balaras E (2008) A Strongly coupled, embedded boundary method for fluid-structure interactions of elastically mounted rigid-bodies. J Fluids Struct 24:167–182
32. Blackburn H, Karniadakis G (1993) Two- and three-dimensional simulations of vortex-induced vibration of a circular cylinder. In: proceedings of the 3rd international offshore and polar engineering conference, Singapore, pp. 715–720